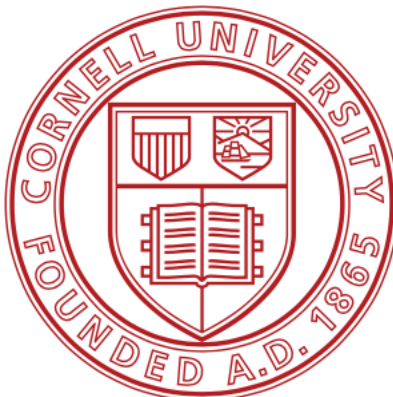


Cornell University



COMPUTER-AIDED ENGINEERING:
APPLICATIONS TO BIOLOGICAL PROCESSES

BEE 4530

Designing and Optimizing a Protocol for Whole-Ovary Vitrification

A Report presented to the Course Staff of BEE 4530 / ENGR 4530 at Cornell University in Partial
Fulfillment of the Requirements for the classes.

Keywords: Ovary Cryopreservation, Vitrification, Cryogenics, Reproduction, Ovary, Numerical Methods

May 22, 2020

Report by:
Mitchell Tyler SCOTT
Dave CHEN
Evan CHENG

Contents

1	Executive Summary	3
2	Introduction	3
2.1	Problem Statement	3
2.2	Design Objectives	5
3	Methods	5
3.1	Schematic	5
3.2	Variables	7
3.3	Governing Equations	8
3.4	Boundary Conditions	9
3.5	Initial Conditions	9
3.6	Computational Methods	9
3.6.1	Numerical Implementation	10
3.7	Assumptions	11
4	Results & Discussion	11
4.1	Mesh Convergence Analysis	11
4.2	Solver Analysis	12
4.3	Study	13
4.3.1	Cryoprotectant Loading	13
4.3.2	Ovarian Vitrification	14
4.4	Validation	14
4.5	Sensitivity Analysis	16
4.6	Optimization	18
5	Conclusion	21

5.1 Conclusion	21
5.2 Future Directions	21
6 Appendices	24
6.1 Input Parameters	24
6.2 CPU Time and Memory used by COMSOL	24
References	25

1 Executive Summary

Ovarian tissue cryopreservation (OTC), a process to preserve human ovarian tissue by cooling to subzero temperature without ice formation, has been increasingly studied within the last 15 years. This is due to the growing scientific capabilities as well as more women who want the procedure for medical or elective reasons. For example, women at or below reproductive age who have to undergo radiological treatments might have to forfeit their fertility. However, if they cryopreserve part or all of their ovary, the ovaries can be reimplanted or *in vitro* fertilization (IVF) can occur to allow fertility options in the future. Other women have been undergoing OTC for more elective reasons such as delaying menopause so that they don't have to live a majority of their life as postmenopausal. There are types of OTC; slow freezing and vitrification. Both require coupled mass and heat transfer. Slow freezing consists of low concentrations of cryoprotective agents (CPAs) which displace water to prevent freezing and a slow cooling rate of about $4^{\circ}\text{C min}^{-1}$. While this is the more thoroughly researched cryopreservation method, research suggests that vitrification is better in the long run, on cellular organelles. Vitrification consists of a higher amount of CPAs present and a cooling rate close to $150^{\circ}\text{C min}^{-1}$. While vitrification has many advantages, there is not a universally agreed-upon standard protocol for vitrification, especially not for the whole ovary. The advantages of OTC on the whole organ would be that upon reimplantation, the hormonal health is assumed to be easily maintained. In order to create a standard vitrification protocol, the criteria for vitrification have to be met (namely the ovary has 6M CPA and then is cooled to -150°C), while then also maximizing the cellular viability. With higher concentration of CPAs especially in vitrification, there is an increase in cytotoxicity, so a cytotoxicity cost function was implemented in aiding the optimization. While creating a 3D computational model of the ovary, with a branched artery and six capillaries, we found that the mesh converged for both heat and mass transfer physics at around 200,000 elements. Using the optimization function, we were able to ascertain that the optimal conditions for the protocol were to submerge the ovary in 9.5 M dimethylsulfoxide (DMSO) for 6 hours and then placed in liquid nitrogen for around 60 seconds. This resulted in a cellular viability prediction of 29.07%, on par with current methods where only parts of the ovaries are cryopreserved. To test the robustness of our model, we varied some of the parameters to see the effect on the protocol. Future directions are analyzed to further improve our model.

2 Introduction

2.1 Problem Statement

The number of women who have considered ovarian tissue cryopreservation (OTC) for medical reasons has increased. In 2018 alone, there were almost 8.3 million new cancer cases in women around the world, and while there are typically speedy diagnoses and treatments, which prolongs the life expectancy for women, the radiological treatments could have a negative effect on a woman's fertility[1, 2]. This can emotionally damage women who were still desiring to have children eventually but now cannot, including adolescents who have never had the opportunity. Without a functional ovary, due to chemotherapy, women can experience hormone imbalances that can cause an increase in heart attack, stroke, osteoporosis, and menopause symptoms[3]. While some patients can go on pharmaceutical hormone replacements, there is no guarantee that the right level of hormones will ever be reached, since every woman is different, and has different endocrinological needs. Also,

the use of pharmaceutical hormone replacements has been linked to an increase in heart attack, stroke, and deep vein thrombosis[4].

There are also more women who are electing for OTC because of an overall increase in life expectancy. While the life expectancy of people is increasing, there has been a trend for women to marry and conceive children later in life . However, the quality of the ovarian follicles decreases considerably with age, so by electing OTC, they can still carry out their wishes and have children later in life without the decreased follicle count and quality. Similarly, because women are living longer, and menopause is occurring at the same time, they are living with the menopause for an increasing percentage of their life. Some women would rather not live 40 years of their life with postmenopausal symptoms such as osteoporosis, heart disease, and depression[5]. By enduring OTC, these women can preserve some of their ovarian follicles, causing a decrease in the duration that they will have to spend postmenopausal [6, 7].

Because there is an increasing demand for OTC, scientific and medical communities need to optimize the cryopreservation and storage of ovarian tissue. There are two standard ways OTC is carried out, slow freezing and vitrification. With slow freezing, the ovarian tissue is removed and cooled at a slow rate to a temperature below its freezing point, then submerged in liquid nitrogen. This slow cooling rate allows for the frozen parts of the tissue to exchange water with the intermembrane space, reducing the number of ice crystals forming in the tissue[8]. However, the reduction of water allows the cells to become hypertonic, which can result in malfunctions in the cell's regulatory systems. While slow freezing is promising because it mitigates some tissue damage by the mechanical stress of freezing water, it has drawbacks by allowing the tissue to undergo hypertonic stress. Cryoprotectants (CPA) can be used to further prevent ice crystal formation and allow water to stay in the tissues[8]. On the other hand, OTC carried out with a fast cooling rate indicative of vitrification of ovarian tissues is dependent on a high concentration of CPAs. This certainly has its drawbacks as well because the high concentrations of CPAs can lead to chemical toxicity, damaging the tissue and hindering the ability for future retransplantation [8]. Vitrification does have many advantages, such as being a quicker process that requires less specialized equipment[9]. Moreover, there are also current studies that have examined methods such as slow freezing and vitrification for preserving ovaries in animals such as zebrafish. The methods were compared by examining factors such as cell membrane integrity, morphology, mitochondrial activity, and DNA damage of the ovaries. Based on the study, it was determined that vitrification was a better method for cryopreserving the ovaries since slow freezing damaged the plasma membrane and mitochondria in the zebrafish ovaries[10, 11].

Slow freezing was once considered the standard in OTC and has many standard protocols[12, 13], but because of more recent studies, there is growing interest in vitrification based OTC. However, because it is newer, there is not yet a standard protocol. In fact, most of the previous vitrification experiments have been performed on individual ovarian follicles or ovarian tissue sections. While the vitrification experiments of the parts of the ovaries show promise, there could be more advantages on a whole-ovary OTC. While simple CPA diffusion will work in the follicles and tissue sections, the whole ovary has the possibility of CPA diffusion and perfusion through the ovarian vasculature. Not to mention, if the whole ovary undergoes vitrification, there will be a higher volume of ovarian follicles. This could allow for either whole ovary retransplantation, or cutting of the vitrified organ, and reimplanting just the follicles[14]. The creation of a standard protocol for whole ovary vitrification can help optimize the process to meet the growing demand for OTC and make the process more efficient. It could also be adapted to other organs, like a kidney, where the whole organ is vital for the function. This could allow for a more efficient organ donation process.

2.2 Design Objectives

The goal is clear: allow for the ovarian tissue to be cryopreserved while minimizing the chemical toxicity associated with CPA loading, resulting in the best chance for retransplantation of a healthy organ. The biggest problem right now is there is no universally agreed upon protocol for ovarian vitrification, especially not for the whole ovary. Without this protocol, there is no way to ensure that chemical toxicity is minimized. By using computer models, this research team investigated the most efficient vitrification protocol. The design objective for this study is to make sure that the whole ovary can be cryopreserved using the least amount of cryoprotectant possible. If too much cryoprotectant is used, the cellular viability is reduced; however, if too little cryoprotectant is used, there is a risk of ice crystal formation within the tissue that will increase mechanical damage and decrease cellular viability. Optimization of ovarian cellular viability is crucial in allowing for fertility. To do this, three parameters need to be balanced to minimize cellular toxicity: the temperature of the tissue, time exposed to cryoprotectant, and concentration of the cryoprotectant. A toxicity model has been developed to minimize chemical and mechanical stress caused by cryoprotectants[15]. This model can be used in accordance with our heat and mass transfer models to calculate what protocol will best optimize cell ovarian cell viability. Although a general universal protocol may be developed, it is important to note that the optimal protocol may vary slightly according to the shape and physical parameters of the ovary, which is investigated in §4.6.

3 Methods

3.1 Schematic

One of the most important features for getting started with computational methods is the geometry over which the math will be calculated. The goal is to balance the physical approximation of the ovary while still making the computations feasible. To get a brief idea of how to implement our computational model into COMSOL , we researched what an ovary looks like.

After initially studying Figure 1, we decided to implement our model into COMSOL as a 2D axisymmetric cylinder as depicted in Figure 2.

This was the model that we used for several early calculations until we saw that the time it took for the CPA to diffuse into our model took close to 11 hours. We thought that the addition of capillaries would be advantageous in our model, but the only way to incorporate capillaries would be to switch to a 3D model. Another advantage of a 3D model is that we reduce the physical approximation error. This would, in turn, reduce our time because we would be able to do branched arteries, and capillaries, while shaving off the points at the top and bottom into a rounder surface. This would also allow us to reduce physical approximation error. The modeling and construction of the 3D model is seen in Figure 3.

Only one-fourth of the ovary is being modelled. This is because when we moved to a 3D geometry, we lost the axisymmetry of the model, but we still had width and depth symmetry. Likewise, since the model is 3D, there would be greater computational complexity as more nodes would be needed to solve for values within

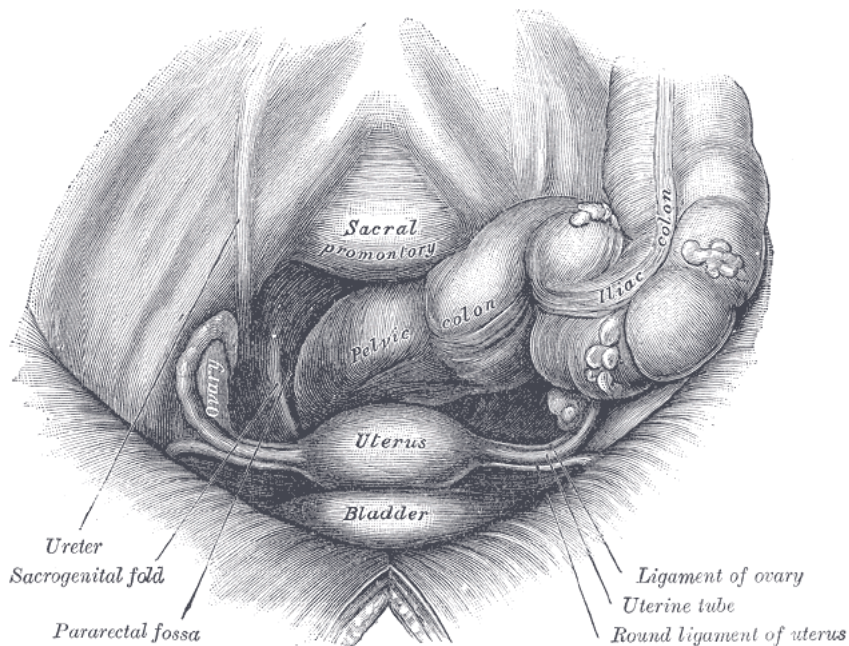


Fig. 1: A Human Ovary. An artist depiction (Gray 1165) of a female reproductive system. The ovary is attached to the uterus and nestled into the *ovarium fossa*. [16].

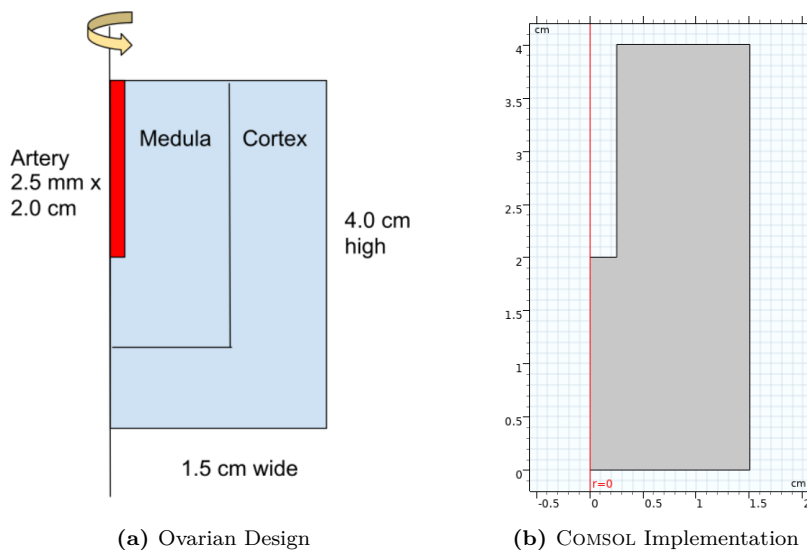


Fig. 2: Creating the 2D ovarian model Stepwise. From researching the ovarian dimensions, the ovarian design (a) was created as a rough sketch of what our model would look like. Taking our design to COMSOL we were able to implement it as shown.

the domain (an option that wasn't applicable with the 2D model). By utilizing the symmetry, we were able to solve for the quarter of the ovary and extrapolate to the entire ovary.

Also, the addition of 6 capillaries was arbitrary. Physically, the ovary has more than six large capillaries, but for a first model of the ovary and balancing the computational feasibility, we decided that six capillaries

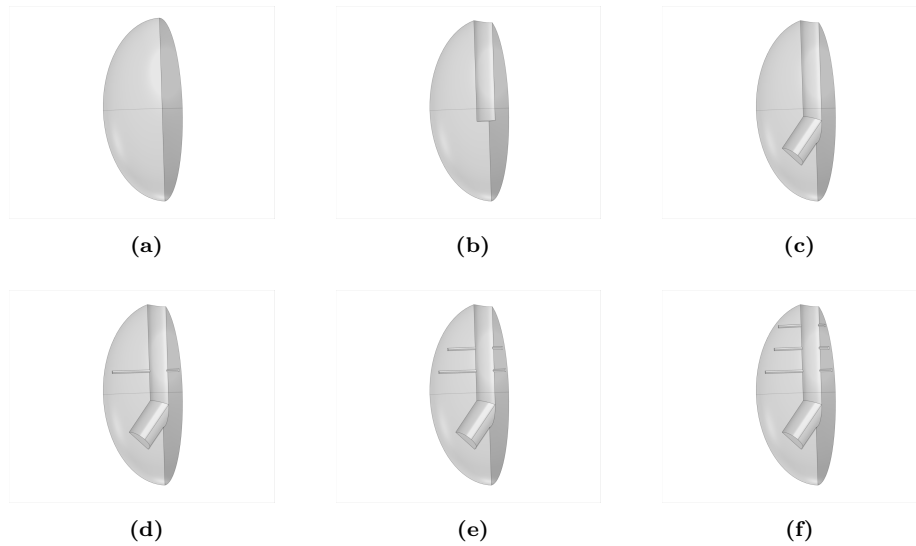


Fig. 3: Creating the 3D ovarian model Stepwise. (a) The start of the 3D model was an ellipsoid. (b) The main ovarian artery is taken out. (c) The ovarian artery becomes branched. (d)-(f) Capillaries are added to make the geometry more realistic.

were a valid approximation. In the end the final geometry was implemented as seen in Figure 4.

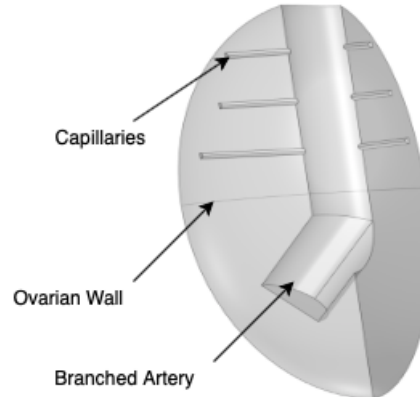


Fig. 4: Final Geometric Model. The final geometry that was implemented into COMSOL . The arrows diagram what the spaces in our geometry physically represent.

3.2 Variables

There are many symbols used within the project, so placing common abbreviations and symbols into a table, we thought the rest of the report would flow smoother (see Table 1). These are the common symbols for heat parameters and diffusion processes.

Table 1: Definition of associated parameters used in the governing equations

Symbol	Units	Description
C_{CPA}	mol m^{-3}	Concentration of cryoprotectant agents
T	K	Temperature
t	s	Time
D_{CPA}	$\text{m}^2 \text{s}^{-1}$	Diffusivity of CPA in the tissue
C_p	$\text{J kg}^{-1} \text{K}^{-1}$	Constant pressure Specific Heat
κ	$\text{W m}^{-1} \text{K}^{-1}$	Thermal conductivity
ρ	kg m^{-3}	Density
\hat{x}	m	distance
\hat{y}	m	distance
\hat{z}	m	distance
E_A	J mol^{-1}	Activation Energy of cell cryodeath
k_∞	unitless	Cryodeath reaction rate at infinite temperature
α	unitless	Kinetic order of CPA/cell death

3.3 Governing Equations

There are two main physics that are happening within the project, transfer of a dilute species and heat transfer in solids. These equations boil down to the same fundamental type of partial differential equation with one time derivative and three spacial derivatives.

The first part of the rapid cooling vitrification is the treatment of the tissue with cryoprotectants. This process is modelled by a mass transfer equation. However, there is an assumption that there is no breakdown of cryoprotectant by the tissue in the region of interest.

The standard diffusion equation assuming there is no reaction term, no conductive or radiative transfer, as well as being angle independent in cylindrical coordinates is given as:

$$\frac{\partial C_{CPA}}{\partial t} = D_{CPA} \left[\frac{1}{r} \frac{\partial}{\partial r} \left(r \frac{\partial C_{CPA}}{\partial r} \right) + \frac{\partial^2 C_{CPA}}{\partial z^2} \right] \quad (1)$$

where $D_{CPA} = 3.02 \times 10^{-10} \text{m}^2 \text{s}^{-1}$ [17]

The standard heat equation assuming no heat source term and no convective heat transfer in cylindrical coordinates is given as:

$$\frac{\partial T}{\partial t} = \frac{k}{\rho C_p} \left[\frac{1}{r} \frac{\partial}{\partial r} \left(r \frac{\partial T}{\partial r} \right) + \frac{\partial^2 T}{\partial z^2} \right] \quad (2)$$

While the formulation started out cylindrically, our model changed to 3D. However, when the equation is being solved in COMSOL , the equation is in Cartesian coordinate since the nodes are classified by (x, y, z)

values. That means that the actual equations that are being solved are

$$\frac{\partial C_{CPA}}{\partial t} = D_{AB} \left(\frac{\partial^2 C_{CPA}}{\partial x^2} + \frac{\partial^2 C_{CPA}}{\partial y^2} + \frac{\partial^2 C_{CPA}}{\partial z^2} \right) \quad (3)$$

$$\frac{\partial T}{\partial t} = \frac{\kappa}{\rho C_p} \left(\frac{\partial^2 T}{\partial x^2} + \frac{\partial^2 T}{\partial y^2} + \frac{\partial^2 T}{\partial z^2} \right) \quad (4)$$

3.4 Boundary Conditions

For the mass transfer, we are subjecting all of the boundaries to a constant concentration boundary condition, where the concentration is between 6.5 and 14 M. This is physically when the ovary is submerged in a vessel with a pump so that fresh CPA is always surrounding the ovary, so the constant temperature can be assumed. The other boundaries are symmetric boundaries where the total domain is cut into 4 identical pieces. These boundaries are zero flux boundaries. Mathematically speaking, these boundary conditions are:

$$\left. \frac{\partial C_{CPA}}{\partial \vec{x}} \right|_{\text{Symmetry Faces}} = 0 \quad (5)$$

$$C_{CPA} \Big|_{\text{Exterior walls and inside arteries and capillaries}} = 6.5M \quad (6)$$

Similarly for the heat transfer boundary condition, we are completely submerging the ovary in liquid nitrogen (ℓN_2). This allows for the fast cooling rate indicative of vitrification. Since ℓN_2 is boiling when the ovary is added, the constant temperature boundary condition can be assumed. These boundary equations were implemented into COMSOL by

$$T \Big|_{\text{Exterior walls and inside arteries and capillaries}} = 77.35K \quad (7)$$

$$\left. \frac{dT}{d\vec{x}} \right|_{\text{Symmetric faces}} = 0 \quad (8)$$

3.5 Initial Conditions

The initial condition of the mass transfer is that the concentration of CPAs especially DMSO is 0 mol m^{-3} . Since DMSO is not naturally made within the human body either directly or as a byproduct, this initial condition assumption is rather feasible. Lastly, the initial condition of the second heat transfer is that the temperature is 277 K. This is the end temperature of the first heat transfer project, and since the diffusion takes place at constant temperature, the temperature should still be the same.

3.6 Computational Methods

In standard OTC protocols, there are three steps, namely the initial cooling of the ovary to the CPA loading temperature, the diffusion/perfusion of the CPA into the ovary, and the cooling step. This implies that the

two equations are one way coupled. The diffusion affects the thermal properties, which in turn affects the heat equation. The initial heating only has to deal with κ, C_p changing as a function of temperature over the range of 37°C to 4°C. During the diffusion step, temperature is being held constant, so the diffusivity is not affected by temperature. However, during the cooling step, there is not only changing temperature, but also a range of different CPA concentrations. This means that κ and C_p need to be functions of both temperature but also concentration.

To find the coupling equations for κ and C_p , we were able to find porcine tissue's thermal properties recorded at varying temperature and CPA concentrations[18]. These 16 values were then able to be made into a least squares problem where there was a constant term, a term dependent on concentration, a term dependent on temperature, and a concentration/ temperature coupling term. The result lead to the coupling equations seen below:

$$\kappa([CPA], T) = -9.33 + 0.002336[CPA] + 0.04082T - 0.00000885[CPA] \cdot T \quad (9)$$

$$C_p([CPA], T) = -1793.3258 + 0.06762[CPA] + 18.8778T - 0.000378[CPA] \cdot T \quad (10)$$

Since we know that κ, C_p have to be nonnegative values, these equations were swept out to every possible value that might be experienced with our model, namely 0-14 M [CPA] and 123.15 - 277.15 K. We saw that the values were all physical within the range that we were interested in. This is because the two biggest terms are positive. When temperature is 123 K, we see that there is a positive value for both κ and C_p

These equations highlight important trends within the vitrification coupling process. Namely, the largest contributor to the changing values in k and C_p was due to temperature. We also see a positive trend in CPA concentration. This makes sense with experimental data where at the same temperature but differing CPA concentration the value of k can be 10-fold different.[19].

3.6.1 Numerical Implementation

The equations are solved using a commercial finite element package, COMSOL Multiphysics Classkit version 5.4 (COMSOL Multiphysics Burlington, MA). Two modules were used in this software: *Transport of Diluted Species* and *Heat Transfer in Solids*. *Transport of Diluted Species* solved the CPA concentration (eq.3). *Heat Transfer in Solids* solved for the initial cooling of the ovary and the vitrification of the ovary (eq.4). A backwards time difference discretization was used with an initial time step of 1 ns. and maximum time step of 1 second was used after. The relative and absolute tolerance values were the default 0.001. A mesh of 238,530 tetrahedral elements was used for the 3D ovary model with a maximum element size of 0.14 cm and minimum elements size of 0.06 cm. Boundary layers were added using the default algorithm with 20 boundary layers and 1.1 growth rate. A Generalized Minimal RESidual method (GMRES) was used with an automatic non-linear iterative solver. Computational run times varied based on the temperature and concentration gradient and ranged from several minutes to several hours with 4 GB RAM and a 64-bit intel Core i3-1005G1 CPU @ 1.20 GHz processor.

3.7 Assumptions

There are a few major assumptions used in simplifying the equations. We assumed that there is no latent heat source term, meaning that the concentration of cryoprotectant was high enough that there was no freezing, and the process was strictly a cooling process.[8]. To make sure that this assumption could be made, we used a lower threshold of 6.0 M CPA concentration everywhere in the ovary to consider the ovary vitrified. Similarly, we used -150°C as the threshold [20, 21].

4 Results & Discussion

4.1 Mesh Convergence Analysis

There are many sources of error that can occur when a physical process has been moved to a computational model— one of which is discretation error. Discretation error occurs when a continuous physical process is now only being evaluated at specific locations called *nodes* and interpolated between the nodes. If there are too few nodes, then the computed values, which recursively rely on the values at each node, differ greatly from the actual solution.

To minimize discretation error, a mesh convergence was performed. Using COMSOL , we ran our problem using different mesh parameters, like the largest and smallest element size. The average concentration within the regime was found for each mesh parameter, which was then converted to the total number of elements. When the average concentration seemed to be independent of number of elements, the mesh was assumed to be converged.

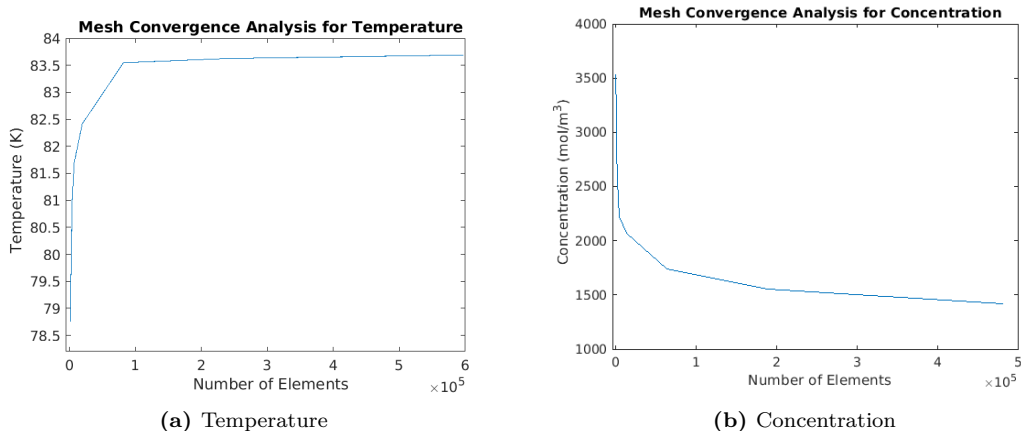


Fig. 5: Visualizing the Average Amount for different Mesh Parameters. Plotting the average temperature and concentration within the model ovary for different meshes, we see that the concentration becomes independent of mesh at around 200,000 elements for both types of physics.

After performing the analysis for concentration, we see that after around 100,000 elements, the average temperature becomes relatively flat, indicating that the answer is independent of the mesh. However, after

around 200,000 elements the average concentration plateaus as seen in Figure 5. This means that the error from discretation has been minimized. Because concentration is an extremely important physical quantity in our model, and we wanted both physics to be independent of the mesh, the mesh used for both physics needs to be over 200,000 elements for our coupled model.

Using COMSOL 's built in mesh algorithm, we created a mesh with the largest element size of 0.14 cm and the smallest element size of 0.6 cm, with a maximum growth rate between the nodes of 1.35. This resulted in a mesh with 150,000. We also then added boundary layers around the capillaries since there is a large concentration gradient between the boundary condition and the interior nodes. This resulted in 230,000 elements, which is above the 200,000 elements needed for the discretation error to be negligible. The final mesh is shown in Figure 6.

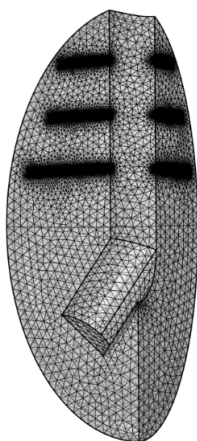


Fig. 6: A fully Converged Mesh. After setting the maximum elements size, minimum element size, and the growth factor, a mesh was created. Through the addition of boundary layers around the six capillaries, the number of elements reached 230,000, so we can assume the mesh is properly converged.

4.2 Solver Analysis

The solver used for the FEM is an important choice and can greatly impact computational speed or memory storage. When trying to Figure out the best solver, there are countless resources like blog posts from COMSOL and other professionals. Once such blog post from Simscale, a competitor of COMSOL , has a road map of which would be the best solver [22]. This blog recommends that this process should be solved by a direct solver since our number of degrees of freedom (265,000) is less than one million. It then recommends that MultFront or MUMPS should be used. However, it is known that direct solvers have a few flaws, namely that they require $\mathcal{O}(n^3)$ time for Gaussian elimination to be computed. Also, sparse matrices (such as the tridiagonal matrix we are using for FEM) cause it to run slowly.

COMSOL automatically picks the best solver for the process at hand to make the process the quickest and most robust. It accomplishes this through analyzing the matrix structure to see if any commonly known structures can be exploited. COMSOL decided that the best solver for this particular model would be an iterative solver using GMRES. To us, it makes sense that we would be using an iterative solver because we are dealing

with half a million degrees of freedom and a sparse tridiagonal matrix. Other than the fact that iterative solvers are not as robust as direct solvers, their answer is always an approximation, albeit an approximation that is continually getting better. This could be tested by comparing the iterations to a calculation done with more iterations. However, the default GMRES solver in COMSOL is iterating 50 times. Even assuming linear convergence of the solver to the correct answer, it makes sense to be around machine epsilon after those 50 steps. Since the most precise thermal or conductive parameter is published with 4 significant Figures, answers do not need to be as precise as 2.2×10^{-16} .

4.3 Study

4.3.1 Cryoprotectant Loading

Obtaining a cryoprotectant concentration above the minimum threshold concentration is critical to minimize cryoprotectant damage. The time to reach the minimal concentration of DMSO is highly dependent on the boundary concentration of DMSO used for perfusion. Figure 7 shows the concentration distribution of DMSO in the ovarian geometry over specified times 6M concentration. Because a 6M concentration of DMSO is required for minimization of cryodamage, our goal was to use the data from the concentration distribution at the minimum time in which each part of the tissue has reached at least a 6M concentration of DMSO. As seen in Figure 7, this occurs between 60000 and 67000 seconds.

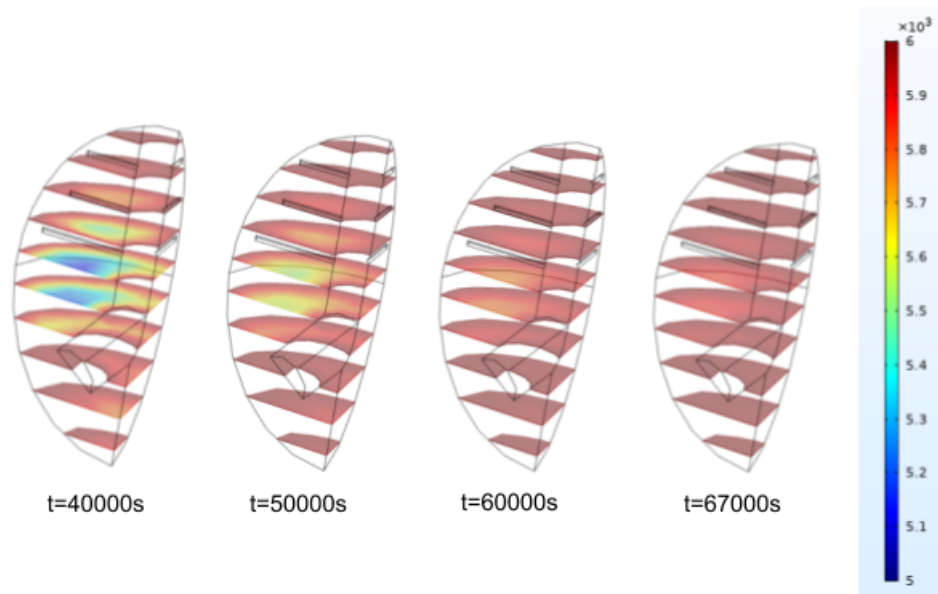


Fig. 7: Diffusion of DMSO into the ovarian model. Using a 6 M boundary condition, we were able to see the ovary increase in concentration over time. At 65,060 seconds, the minimum assumed requirement for vitrification was met.

Although a 6M concentration was used for our initial analysis, our results from the optimization analysis indicate that a 9.5M initial concentration of DMSO is optimal for cell viability. The mass transfer process was done for a 9.5M boundary condition and is shown in Figure 8. As seen in Figure 8, a 6M concentration within

the whole ovarian geometry is achieved between the 22,000 and 24,000 mark. The duration of DMSO exposure is significantly lower using a 9.5M DMSO concentration for perfusion and is likely the most significant reason that it offers a greater cell viability when compared to the 6 M boundary condition.

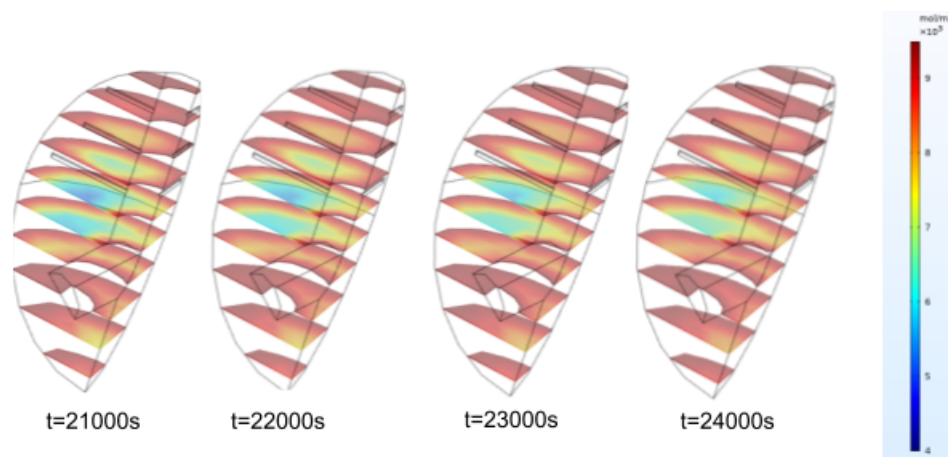


Fig. 8: Optimal Concentration for Diffusing DMSO into the Ovary. Using a 9.5 M boundary condition, we were able to see the ovary increase in concentration over time. At 24680 seconds, the minimum assumed requirement for vitrification was met. Since the legend only has finite colors but the range covers more values, the differences in concentration may be harder to see.

4.3.2 Ovarian Vitrification

Following the loading of cryoprotectants, ovarian vitrification will occur. Before vitrification begins the tissue will be at a temperature of 277K. The ovarian tissue will be submerged and continuously perfused with liquid nitrogen. Liquid nitrogen has a temperature of 77K and the perfusion will continue until each region of the ovarian geometry reaches 123K, the minimum temperature for vitrification to be viable. As seen in Figure 9, this occurs at 49 seconds.

4.4 Validation

The first step to validation would be to compare what we have to the analytical solution, since this is a continuously defined answer. However, our model would differ greatly from the analytical solution for many reasons, namely our domain isn't in rectangular, cylindrical, or spherical coordinates, the only domains where there is a well defined analytical solution. Our model also uses varying thermal parameters, and anisotropic materials. This is another reason that the analytical solution wouldn't give us a strong validation.

The next step for validation would be if there were any experimental procedures for human OTC, which there is not. Finally, a form of validation might have to come from experimental procedures from any ovarian tissue. While this is not ideal, Choi and Bischof (2008)[23] do state that since human ovarian tissue thermal values during OTC are scarce, other tissues such as porcine liver and porcine ovary tissue in the literature are more prevalent and the trends follow the same trend for all human ovarian tissues. Furthermore, there

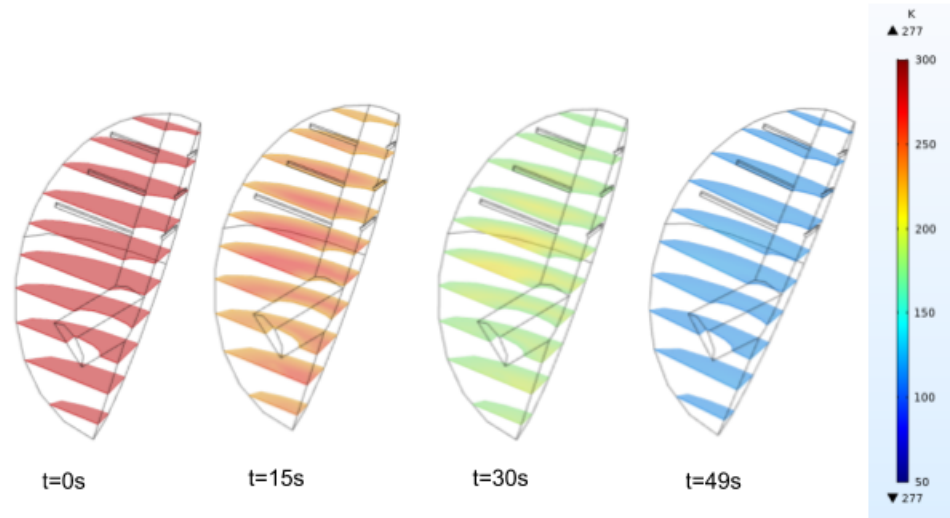


Fig. 9: Final Cooling Rate of the Protocol. Once the ovary had reached the concentration threshold, the fast freezing could begin. The ovary was dipped in ℓN_2 and because of the very large temperature gradient, the ovarian model reached -150°C after 50 seconds.

is no data on the concentration of cryoprotectant at a specific location in the ovary. There are no published studies on the measurement of temperature at specific locations in the whole ovary either. However, there have been published studies on the mass transfer of cryoprotectant in a slab of ovarian tissue[24]. Our approach simulated their experimental procedures by using the mass transfer coefficients used in the 3D whole ovary. The study done by Han *et. al* used spectroscopic monitoring to determine transport processes during loading of ovarian tissue with cryoprotective solutions[24]. In this study, thin pieces of cylindrical ovarian pieces were incubated in solution containing CPA. CPA permeation into porcine ovarian tissue was then determined using an osmometer to measure osmolality. The results of the concentration of DMSO as a function of position for the experimental ovarian tissue slice. This is shown in Figure 10. Although our 3D model cannot be compared with this experimental procedure, we used our diffusivity and mass transfer coefficients to simulate their experiment to determine if our model is reasonable.

We see that our model's diffusion seems to be matched closely with the experimental results. However, our model uses a CPA diffusivity that is about 45% less than the value that they used. This is most clearly seen in the 60 minute panel[24]. After 60 minutes, their model has a minimum concentration near the axis of symmetry of about 5.5 M; whereas, our model at the same time and location, has a minimum concentration of 4.5M. The reason behind this difference in CPA diffusivity is that depending on which spectroscopic method that Han used, the diffusivity value would vary up to one order of the magnitude from the smallest to the largest value they reported. Because of this large range, we decided to use a value that was an average of all the values presented in this paper.

While we see that visually our validation gets close to experimental results in Figure 11, the rate of increase in average CPA concentration within the ovarian tissue cylinder of our model matches very closely with the experimental values. The concentration was normalized so as to see the percent of the highest concentration change over time.

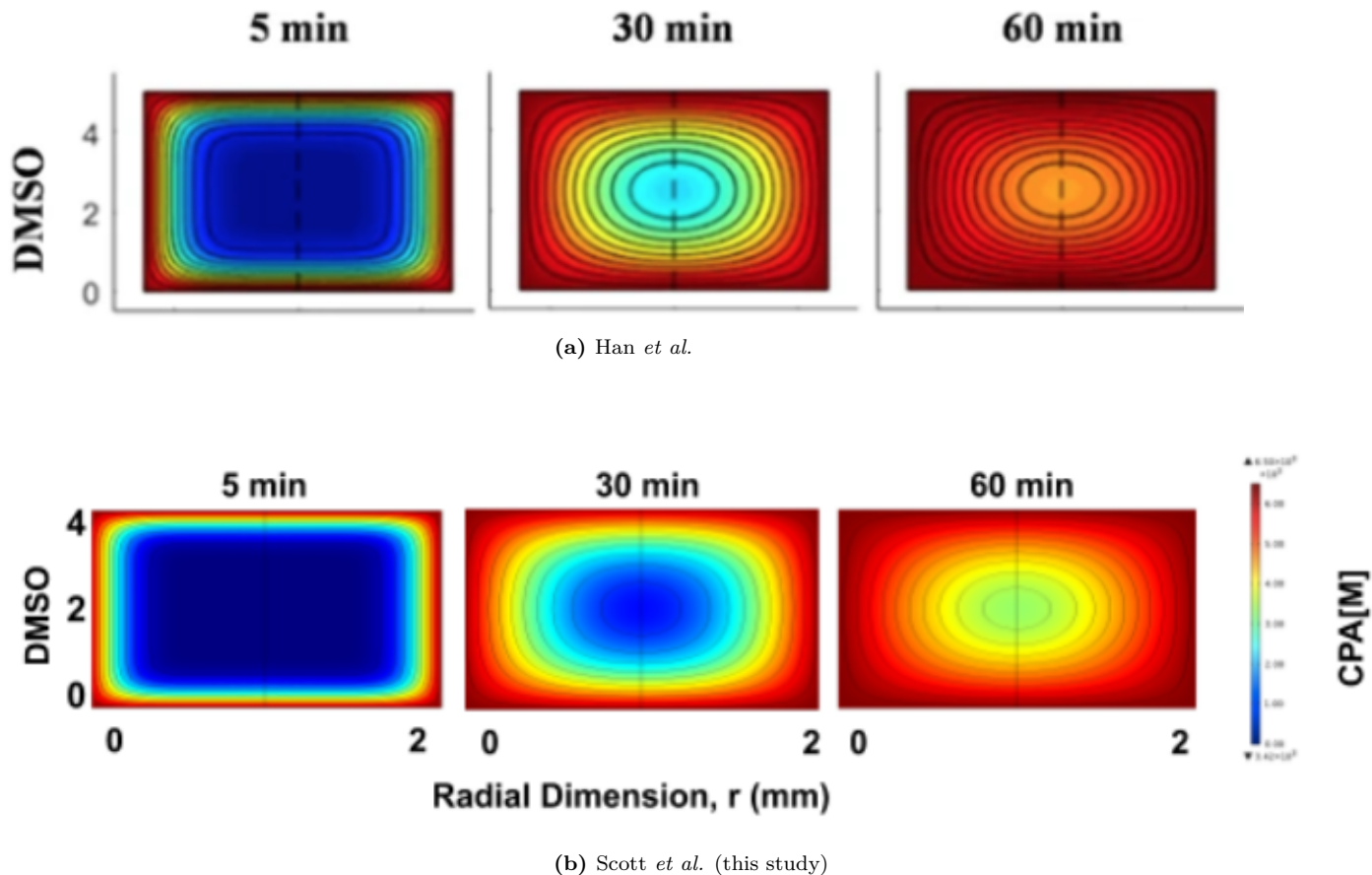


Fig. 10: Comparing the Concentration of CPA to Experimental Results. Comparing to Han *et al.*, we see that our model matches closely to their model with the main source of error as a different value for diffusivity. Our model is compared to the data, namely at time 5, 30, and 60 minutes.

The Han study only took discrete values at 0, 5, 30, and 60 minutes. These values were superimposed onto our plot to see the relationship. We see that our model seems to diffuse slower than experimental data at smaller times, but at larger times our model seems to surpass those found by Han, but they were always within one standard deviation of Han’s values. One of the reasons our model seems to increase more than experimental results at long times is due to normalization. Within the paper, Han never discusses what value was used to normalize the average concentration. Based on the concentration curve, we assumed it was when the entire ovary was in species equilibrium; however, for our model we used the average concentration at 60 minutes to normalize our data. This explains why the last value for us is 1 and theirs is 0.96.

4.5 Sensitivity Analysis

After a thorough literature review, the values for human ovarian thermal parameters such as κ and C_p were extremely hard to find, let alone ovarian tissue parameters that varied depending on temperature and CPA concentration. However, these parameters are the crux of the vitrification phenomena, so simply excluding these properties would make our computational model in no way representative of the actual physics..

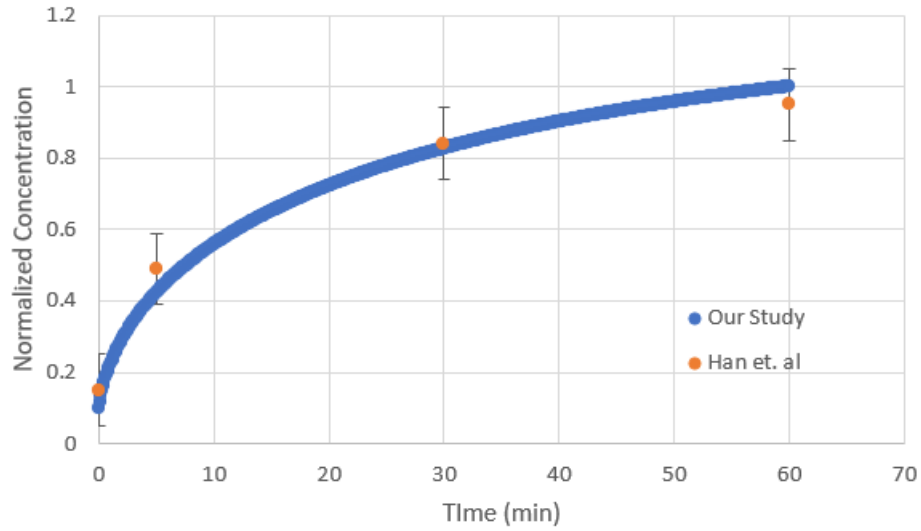


Fig. 11: Validation the Diffusion of our Model compared to Experimental data[24]. The blue curve was the average concentration percentage in our ovarian cylinder as a function of time. The orange data points with the error bars are Han’s model. It is seen that our model has the same concentration increase rate.

Values for our major input parameters were increased by $\pm 10\%$ to see the effect the parameters found in literature, which might be slightly different or inaccurate for our model, could have on the overall protocol. For the mass transfer, the only parameter that we varied was the diffusivity. We were advised that instead of increasing by 10%, a more robust solution would come if diffusivity was varied by one order of magnitude.

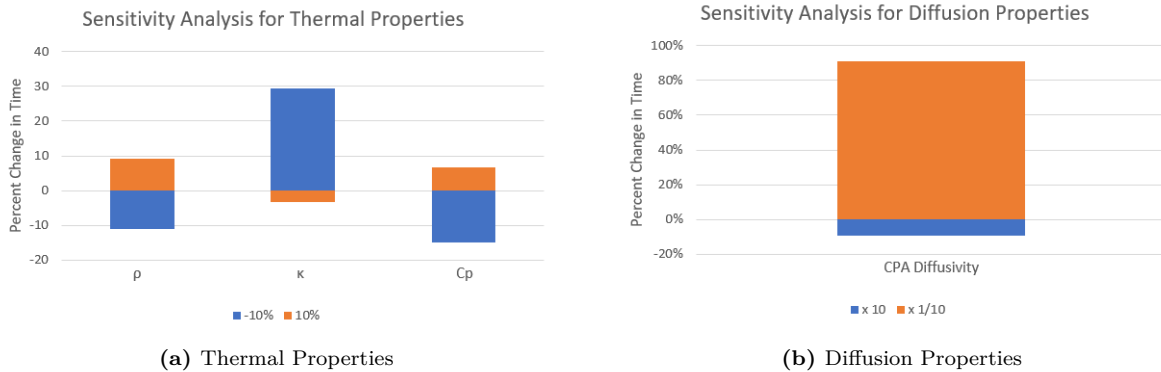


Fig. 12: Sensitivity Analysis of Thermal and Diffusive Parameters. (a) Sensitivity analysis was carried out by varying the thermal parameters (ρ , κ , and C_p) by $\pm 10\%$ to assess how this would effect the system overall. (b) Sensitivity analysis was carried out by varying the diffusive parameter D_{AB} by $10^{\pm 1}$ to assess how this would effect the system overall.

For thermal properties, we altered ρ , κ , and C_p . This is because these values are very important in determining the dynamics of the partial differential equations. We see from increasing ρ and C_p the amount of time that it takes to reach the temperature threshold decreases. For the heat equation $\alpha = \frac{\kappa}{\rho C_p}$, so by increasing ρ or C_p , we are decreasing α , which means the new model will take more time compared to our base

model. Conversely, since κ is directly proportional to α , an increase in κ would increase the thermal diffusivity, which reduce the time needed to reach the threshold condition. This is exactly what we see in Figure 12 for the thermal properties.

This mathematical analysis fits the diffusion property of concentration diffusivity. Like α in heat transfer, D is the diffusivity for mass species. We see the same trend. If we increase diffusivity, then the time needed to reach the threshold conditions would decrease, showing a negative percent change in time. Conversely, decreasing the diffusion means that it will take longer for the diffusion to occur, so more time.

4.6 Optimization

Cryoprotectants (CPAs) can be toxic to cells because the CPAs are forcing the water out of the cell, and cells need water to continue living. CPA cytotoxicity is dependent on the concentration of the CPA within the cells, the duration the CPA is in the cell, the temperature at which CPA loading occurs, and the types of CPAs present, as some CPAs are more toxic than others. Since we have found multiple reports that indicate that DMSO is the most effective CPAs for vitrification, [25] our model only uses DMSO. We also assumed that the CPA loading temperature would be constant[11]. This means that our cytotoxicity model only needs to depend on concentration and duration of the CPA in the ovary. Such a model was found; using a power law equation for cytotoxicity and an Arrhenius dependence on temperature, the following cytotoxicity cost function was established[26]:

$$J = \int_0^{t_f} k_{\infty} e^{\left(\frac{-E_A}{RT}\right)} (C_s^i)^{\alpha} dt \quad (11)$$

where t_f is the protocol duration, k_{∞} is the rate constant at infinity temperature, E_A is the activation energy of cell death, R is the universal gas constant, and α is the assumed order of the reaction.

This cost function was then linked to the ratio of viable tissue after the protocol by the following equation:

$$\frac{N_f}{N_i} = e^{-J} \quad (12)$$

This calculation was carried out on a single cell, so to implement this into our computational model, we took the average concentration over the entire ovary at a time and then took the time integral of the average concentration curve.

$$J = \int_0^{t_f} (C_{CPA,avg})^{\alpha} dt \quad (13)$$

Using this model, the average concentration over time was calculated for varying boundary conditions. Since the goal of this project was to find the optimal protocol, the external boundary condition concentration was varied between 6 and 14 M DMSO in 0.5 M increments. Since we assumed that every cell had to have a CPA concentration of 6M to be considered vitrified, it didn't make sense to use values for the boundary condition below 6M. Similarly, 100% DMSO is approximately 14M, so the value couldn't be higher than that. The goal of changing the boundary condition would be to find the minimum in the concentration versus duration trade-off.

Obviously, the lower concentration would be less toxic to the cell but would take longer, which is damaging to the cell. Conversely, the higher concentration of boundary condition would take less time but the concentration would be more damaging.

Once the average concentration within the ovary was found as a function of time for each boundary condition, the J value was found by numerically integrating the $C_{CPA,avg}$ over the time it took the concentration to meet the threshold at all parts of the ovary. Using the parameters values $\alpha = 1.6$, $k_{\infty} = 10^7$, and $E_A = 36000\text{J mol}^{-1}$, we were able to get the cost function for each boundary condition to find the minimum value[27, 28].

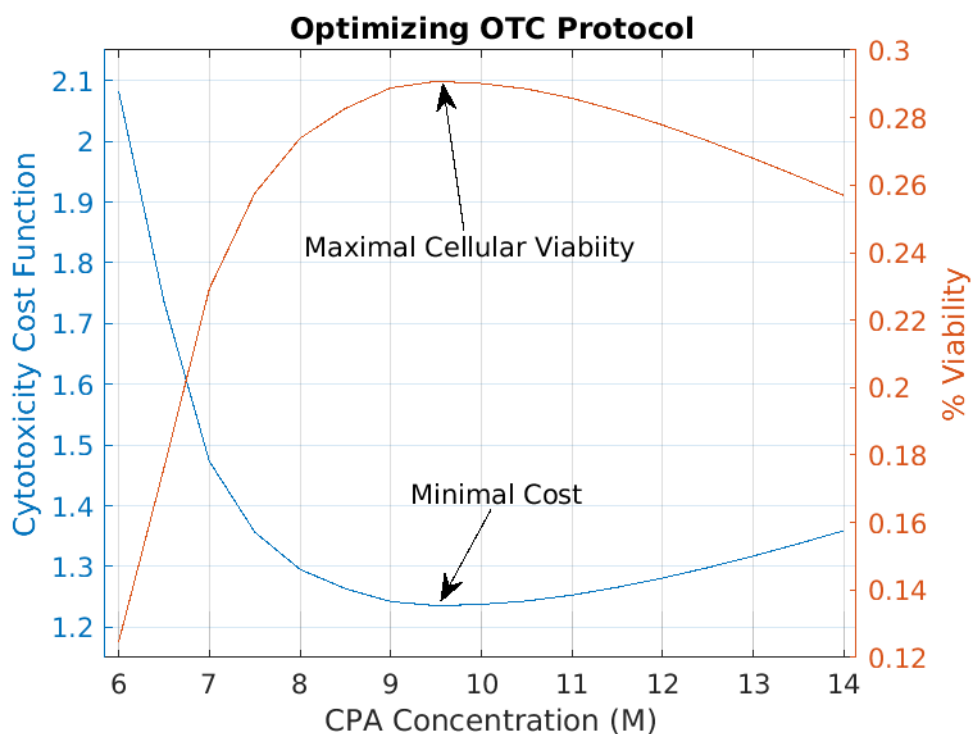


Fig. 13: Visualizing the Cost Function and Cellular Viability. The cost function and the cellular viability changing based on the CPA concentration of the boundary condition.

As Figure 13 shows, there is a minimum cost function value of about 1.25. The minimal cost function value corresponds to the maximal cellular viability by equation 13. We see that by carrying out our protocol using 9.5 M DMSO to perfuse/diffuse into the ovary, about 29% of the ovary will still be viable for reimplantation.

To get the values for the optimization, we assumed that the values for α , k_{∞} , and E_A were those presented in the paper where we found the model. However, these values are all best fit approximation values for the epithelial cells. Since we are using ovarian cells, a sensitivity analysis for those three parameters were performed.

The smallest variability in viability comes from changing k_{∞} . By decreasing k_{∞} 20%, the viability decreased by 28%. Similarly, by increasing k_{∞} by 20% the viability increased by 21%. This close to linear relationship has to do with the fact that we are scaling the entire cost function, J , but the actual quantity we care about is $\exp\{-J\}$. It also makes sense that as we increase the percentage, the viability percentage

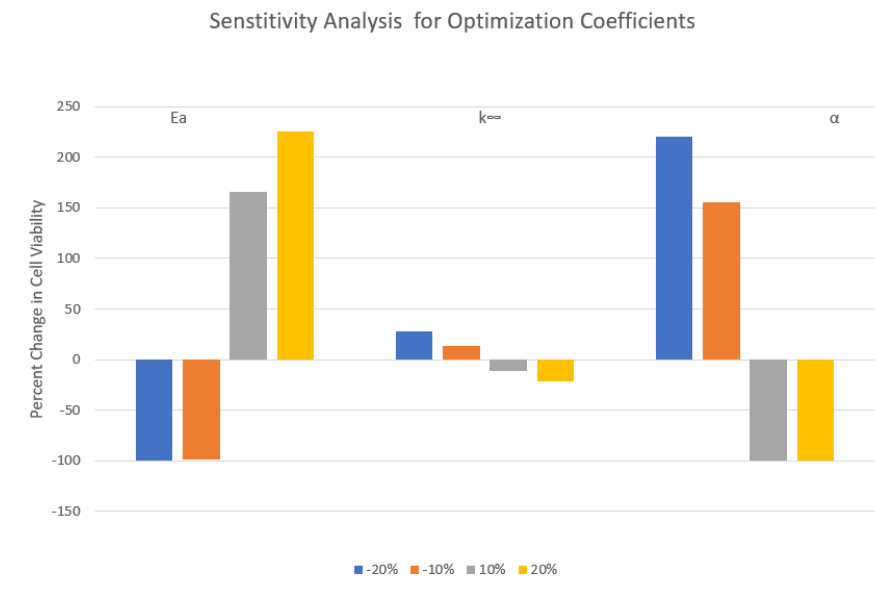


Fig. 14: Optimization Sensativity Analysis. By varying the parameters of E_A , k_∞ , and α all by $\pm 10\%$ and $\pm 20\%$, the percent change in cellular viability is seen. E_A and α cause quite a bit of difference in our cell viability model by changing them only slightly. However, the k_∞ parameter seems to only nomially affect the vaibility projection.

decreases, for $\exp\{-\text{Larger Value}\} = 1/\exp\{\text{Larger Value}\}$ so the value will be smaller. The other two values see great vicissitudes when changing the input parameter. This is because E_A and α are directly and inversely proportional the exponential function, respectively. Physically, if E_A increases then the energy required to kill the cell increases, so with the same amount of energy in the system, fewer cells can die. If E_A increases $\exp\{-E_A/RT\}$, then J will be exponentially smaller, so cell viability will be exponentially larger. Conversely, if α increases that means the kinetics of the rate law happen faster, so more cells will die, meaning the viability will be lower, as seen by Figure 14.

Since the values for these parameters are most likely different for the ovarian cells as compared to the epithelial cells, these values need to be well known to ensure the model properly predicts the viability of our process.

For our optimization of the process, the diffusion doesn't follow an analytical function, so to find the value under the $(C_{avg})^\alpha$ curve over time, numerical integration was used. There were some error associated with this method. First, there was some error with the data exported from COMSOL . At short time steps, the average concentration within the ovary didn't make sense. At time zero, the initial condition is still in effect so the average at time zero should be 0 mol m^{-3} , but this value was anywhere from 700 to 2000 mol m^{-3} .

Another potential source of error within the model would be the trapezoidal numerical integration. Trapezoidal is one of the best discrete numerical integration procedures, but it is not the total area unless the number of trapezoids go to infinity with the width approaching zero. Because of this the value for J , the cost function, was always under reported. While this surely isn't a large source of error for deciding which was the optimal boundary condition, especially since all of the different boundary conditions for the optimization

underwent the same procedure, this under-reporting for J could have large effects on the viability calculations since as we have shown in Figure 14, the that changing J slightly can have an exponential decrease in terms of the viability.

One of the largest assumptions that we made in terms of the optimization was that the perfusion/diffusion was performed at constant temperature, and the cytotoxicity function only involved the diffusion and not the rapid cooling step. This was because a vast majority of the procedure involves the perfusion/diffusion, so the last 60 seconds, when the temperature change occurs, is negligible. This further reduced the J value compared to its actual amount. The integral was evaluated from time zero to whenever the concentration threshold was met. While the lowering of the temperature would have reduced the Arrhenius part of the integral, that extra area under the curve is not being accounted for. This assumption for computational ease, could greatly effect the cost function and effect the cellular viability. Also, another reason the changing temperature term should be added is because once the CPA is in the ovary, there is no reaction to remove it. The value will stay constant or further increase during the cooling part of the protocol.

5 Conclusion

5.1 Conclusion

Through the project our goal was unwavering: design a whole ovary vitrification protocol. We systematically reduced error from physical approximation error to discretation error to iterative convergence error. The final result was a whole-ovary cryopreservation protocol. Once the ovary is surgically removed from the patient, it is immediately cooled down in a medical refrigerator at -20°C for approximately 2 minutes. Once the ovary reaches 4°C , 9.5M DMSO is perfused/diffused into the ovary at a constant temperature in a swirling container to assume constant concentration. After about 6 hours, the ovary was properly treated with CPA as to not freeze. It was then placed in liquid nitrogen for 60 seconds until the maximum temperature within the ovary was no more than -150°C . The ovary is then stored in a medical cooler until reimplantation or IVF is so desired.

5.2 Future Directions

One of the largest sources of error for this project is the physical approximation error. This manifests in the geometry that was used. The ovary was assumed to only have one large central ovarian artery, with a few smaller capillaries jetting straight out of the central artery. This model works for a preliminary study of the ovary, but the actual vasculature of the organ is more complicated than our preliminary project. The arteries branch off at various angles with tapered ends and are more in number than six arteries. This physical approximation error causes the perfusion of the CPA to take much longer than it actually would, which causes the cell viability calculation and optimization algorithm to be off. When comparing to the previously conducted experimental protocols, this causes our protocol to look unreasonable.

To get an accurate geometry, the most efficient and accurate procedure would be to take human ovaries and take MRI or CT scans of the ovary as a whole as well as slices of the organ.[29] This could then be processed

through several softwares that allow for the smoothing of the mesh, combination of the individual meshes, and the ability to differentiate arteries, capillaries, veins, follicles, and different tissue types (medullar or cortex). This process was estimated to take three to four months, which was not feasible for our project timeline. It should further be noted that the results would be novel as there are no open source online ovaries geometries on major databases. Continuing with this geometry formation would not only reduce the physical approximation error in our report, but it would help the countless researchers who come after us to get the most accurate results.

The parameters that were used for this project would also need to be improved if this project were to continue. Through an extensive literature review, there were no values for thermal or diffusion related parameters in human ovaries found, and worse yet, very limited porcine or bovine ovarian parameters that were functions of temperature and CPA concentration. This forced us to use approximate values found from porcine livers in some cases. This problem however is a rather easy fix. Given access to a wet lab, the thermal and diffusive properties of human ovarian tissue can be studied. This will give a more nuanced view of how the parameters are affected by temperature and CPA concentration. While ideally there would be an analytical function that would only be dependent on those two parameters, just getting more data points would allow for a better least squares approximation for the parameters. This would mean that our model is more accurate and allow the optimization algorithm to find a more accurate protocol for whole organ OTC.

One main assumption that going forward would be to allow for the change in density as a function of temperature but namely CPA concentration. The whole purpose of a CPA is to displace water and take its place. When freezing comes around, the water is gone and cannot freeze and cause ice related damage. However, DMSO doesn't have the same volume as water, so as DMSO displaces the water, the volume and density of the ovary is changing. The swelling of the ovary allows for different stresses and can effect the diffusion rate of ovarian tissue. Namely, since water is more dense then DMSO, when water leaves, the tissue will shrink which will for a short time allow the DMSO to diffuse quicker since the tissue is more porous, but then when the DMSO fully replaces water, the tissue will be stretched which can affect thermal properties [30].

As seen by Westphal, the minimal threshold that was used of 6M for the concentration seems to be too high[31]. When looking for the threshold value, we found a range of 3.5 - 6M was the requirement for vitrification. To make sure that we could assume there was no latent heat for within the system, we collective agreed to use 6M as the requirement. As more research is done in the field of OTC, there are novel designs that allow vitrification to happen by using lower concentration thresholds like 2 M. Since this process was entirely computational and no we lab experimentation took place, there was no easy was to know if the model vitrified; whereas, in the lab if the ovary becomes glossy, it is assumed to be properly vitrified. In an attempt to guarantee that our model was vitrified, we set the thresholds too high, especially in terms of concentration. Going forward, we will assume that the model is vitrified at 2.5 M everywhere within the ovary.

While our model is far from the most accurate physical process that is occurring, it is a great first attempted at computationally modelling the human ovary in a cryogenic regime. The lack of quality ovarian models being used in scientific research is appalling. By trying to bridge the gap in understanding between what happens in male bodies compared to female bodies, this sort of research is a great first step. These models can be expanded to other organ systems for the likes of organ donation. Being able to allow for cryogenically preserved organs in a healthy manner for re-implantation can help solve the organ and blood shortages that

America faces, especially in times of global pandemic like we are currently experiencing.[\[32\]](#).

6 Appendices

6.1 Input Parameters

Table 2: Thermal and Diffusive properties of human ovarian tissue.

Parameter	Symbol	Value	Units	Source
Human Ovarian Tissue Properties				
Diffusivity	D_{AB}	3.02×10^{-10}	$\text{m}^2 \text{s}^{-1}$	[17]
Density	ρ	1048	kg m^{-3}	[33]
Specific Heat	C_p	3778	$\text{J kg}^{-1} \text{K}^{-1}$	[18]
Thermal Conductivity	κ	0.56	$\text{W m}^{-1} \text{K}^{-1}$	[18]

6.2 CPU Time and Memory used by Comsol

```

Time-stepping completed.
Solution time: 6238 s. (1 hour, 43 minutes, 58 seconds)
Physical memory: 1.35 GB
Virtual memory: 8.75 GB
Ended at May 16, 2020 3:46:17 PM.
----- Time-Dependent Solver 1 in Study 1/Solution 1 (soll) ----->
=====
===== Opened BEE4530_Ovary vitrification_Mayuri.mph =====

```

References

- [1] “Worldwide cancer data,” Aug. 2018. Library Catalog: www.wcrf.org.
- [2] M. Vassilakopoulou, E. Boostandoost, G. Papaxoinis, T. de La Motte Rouge, D. Khayat, and A. Psyrri, “Anticancer treatment and fertility: Effect of therapeutic modalities on reproductive system and functions,” *Critical Reviews in Oncology/Hematology*, vol. 97, pp. 328–334, Jan. 2016.
- [3] “Overview | Fertility problems: assessment and treatment | Guidance | NICE.” Library Catalog: www.nice.org.uk Publisher: NICE.
- [4] J. Marjoribanks, C. Farquhar, H. Roberts, and A. Lethaby, “Long term hormone therapy for perimenopausal and postmenopausal women,” *Cochrane Database Syst Rev*, p. CD004143, July 2012.
- [5] C. A. Amorim, “Cryopreservation of oocytes from pre-antral follicles,” *Human Reproduction Update*, vol. 9, pp. 119–129, Mar. 2003.
- [6] K. Christensen, G. Doblhammer, R. Rau, and J. W. Vaupel, “Ageing populations: the challenges ahead,” *Lancet*, vol. 374, pp. 1196–1208, Oct. 2009.
- [7] “Life Expectancy - Our World in Data.”
- [8] P. Mazur, “Freezing of living cells: mechanisms and implications,” *Am. J. Physiol.*, vol. 247, pp. C125–142, Sept. 1984.
- [9] G. M. Fahy, D. R. MacFarlane, C. A. Angell, and H. T. Meryman, “Vitrification as an approach to cryopreservation,” *Cryobiology*, vol. 21, pp. 407–426, Aug. 1984.
- [10] L. S. Marques, A. A. N. Fossati, R. B. Rodrigues, H. T. Da Rosa, A. P. Izaguirry, J. B. Ramalho, J. C. F. Moreira, F. W. Santos, T. Zhang, and D. P. Streit, “Slow freezing versus vitrification for the cryopreservation of zebrafish (*Danio rerio*) ovarian tissue,” *Scientific Reports*, vol. 9, pp. 1–11, Oct. 2019. Number: 1 Publisher: Nature Publishing Group.
- [11] Q. Shi, Y. Xie, Y. Wang, and S. Li, “Vitrification versus slow freezing for human ovarian tissue cryopreservation: a systematic review and meta-analysis,” *Scientific Reports*, vol. 7, pp. 1–9, Aug. 2017.
- [12] R. G. Gosden, D. T. Baird, J. C. Wade, and R. Webb, “Restoration of fertility to oophorectomized sheep by ovarian autografts stored at -196 degrees C,” *Hum. Reprod.*, vol. 9, pp. 597–603, Apr. 1994.
- [13] D. A. Gook, D. H. Edgar, and C. Stern, “Effect of cooling rate and dehydration regimen on the histological appearance of human ovarian cortex following cryopreservation in 1, 2-propanediol,” *Hum. Reprod.*, vol. 14, pp. 2061–2068, Aug. 1999.
- [14] S. Yavin and A. Arav, “Measurement of essential physical properties of vitrification solutions,” *Theriogenology*, vol. 67, pp. 81–89, Jan. 2007.
- [15] A. Bhattacharya and R. L. Mahajan, “Temperature dependence of thermal conductivity of biological tissues,” *Physiol Meas*, vol. 24, pp. 769–783, Aug. 2003.
- [16] “Ovary | animal and human.” Library Catalog: www.britannica.com.

- [17] A. Vásquez-Rivera, K. K. Sommer, H. Oldenhof, A. Z. Higgins, K. G. M. Brockbank, A. Hilfiker, and W. F. Wolkers, “Simultaneous monitoring of different vitrification solution components permeating into tissues,” *Analyst*, vol. 143, no. 2, pp. 420–428, 2018.
- [18] J. Choi and J. Bischof, “Review of biomaterial thermal property measurements in the cryogenic regime and their use for prediction of equilibrium and non-equilibrium freezing applications in cryobiology,” *Cryobiology*, vol. 60, pp. 52–70, Feb. 2010.
- [19] M. A. Nowshari, P. L. Nayudu, and J. K. Hodges, “Effect of cryoprotectants and their concentration on post-thaw survival and development of rapid frozen-thawed pronuclear stage mouse embryos,” *Hum. Reprod.*, vol. 10, pp. 3237–3242, Dec. 1995.
- [20] J. G. Baust, D. Gao, and J. M. Baust, “Cryopreservation,” *Organogenesis*, vol. 5, no. 3, pp. 90–96, 2009.
- [21] C. A. Amorim, P. B. D. Gonçalves, and J. R. Figueiredo, “Cryopreservation of oocytes from pre-antral follicles,” *Hum. Reprod. Update*, vol. 9, pp. 119–129, Apr. 2003.
- [22] M. V. K. Chari and S. J. Salon, “3 - THE FINITE DIFFERENCE METHOD,” in *Numerical Methods in Electromagnetism* (M. V. K. Chari and S. J. Salon, eds.), Electromagnetism, pp. 105–141, San Diego: Academic Press, Jan. 2000.
- [23] J. Choi and J. Bischof, “A quantitative analysis of the thermal properties of porcine liver with glycerol at subzero and cryogenic temperatures,” *Cryobiology*, vol. 57, pp. 79–83, Oct. 2008.
- [24] J. Han, B. Sydykov, H. Yang, H. Sieme, H. Oldenhof, and W. F. Wolkers, “Spectroscopic monitoring of transport processes during loading of ovarian tissue with cryoprotective solutions,” *Scientific Reports*, vol. 9, p. 15577, Oct. 2019. Number: 1 Publisher: Nature Publishing Group.
- [25] M. Dattena, C. Accardo, S. Pilichi, V. Isachenko, L. Mara, B. Chessa, and P. Cappai, “Comparison of different vitrification protocols on viability after transfer of ovine blastocysts in vitro produced and in vivo derived,” *Theriogenology*, vol. 62, pp. 481–493, Aug. 2004.
- [26] A. F. Davidson, C. Glasscock, D. R. McClanahan, J. D. Benson, and A. Z. Higgins, “Toxicity Minimized Cryoprotectant Addition and Removal Procedures for Adherent Endothelial Cells,” *PLOS ONE*, vol. 10, p. e0142828, Nov. 2015.
- [27] A. F. Davidson, C. Glasscock, D. R. McClanahan, J. D. Benson, and A. Z. Higgins, “Toxicity Minimized Cryoprotectant Addition and Removal Procedures for Adherent Endothelial Cells,” *PLoS One*, vol. 10, Nov. 2015.
- [28] J. D. Benson, A. Z. Higgins, K. Desai, and A. Eroglu, “A toxicity cost function approach to optimal CPA equilibration in tissues,” *Cryobiology*, vol. 80, pp. 144–155, 2018.
- [29] A. Pagès, M. Sermesant, and P. Frey, “Generation of computational meshes from MRI and CT-scan data,” *ESAIM: Proc.*, vol. 14, pp. 213–223, Sept. 2005.
- [30] R. V. Devireddy, “Predicted permeability parameters of human ovarian tissue cells to various cryoprotectants and water,” *Molecular Reproduction and Development*, vol. 70, no. 3, pp. 333–343, 2005.

- [31] J. R. Westphal, R. Gerritse, D. D. M. Braat, C. C. M. Beerendonk, and R. Peek, “Complete protection against cryodamage of cryopreserved whole bovine and human ovaries using DMSO as a cryoprotectant,” *J Assist Reprod Genet*, vol. 34, pp. 1217–1229, Sept. 2017.
- [32] E. B. Finger and J. C. Bischof, “Cryopreservation by vitrification: a promising approach for transplant organ banking,” *Curr Opin Organ Transplant*, vol. 23, no. 3, pp. 353–360, 2018.
- [33] J. O. Karlsson, E. A. Szurek, A. Z. Higgins, S. R. Lee, and A. Eroglu, “Optimization of Cryoprotectant Loading into Murine and Human Oocytes,” *Cryobiology*, vol. 68, pp. 18–28, Feb. 2014.

Table 3: Thermal properties of biological tissues and materials in the subzero temperature domain.

Material	Thermal Conductivity [$\text{W m}^{-1} \text{K}^{-1}$]	Specific Heat [$\text{J g}^{-1} \text{K}^{-1}$]	Latent Heat (ice) [J g^{-1}]	Source
Porcine Liver	1.6 (-11°C)	3.659 (0°C)	223.4	[18]
	1.75 (-64°C)	1.522 (-73°C)		
	1.9 (-112°C)	1.192 (-109°C)		
	2.0 (-147°C)	0.941 (-147°C)		
Porcine Liver treated with 1xPBS, 2 M glycerol	1.56 (-10°C)	3.394 (-4°C)	146.4	[18]
	1.68 (-64°C)	1.611 (-73°C)		
	1.78 (-108°C)	1.135 (-109°C)		
	1.73 (-146°C)	0.872 (-147°C)		
Porcine Liver treated with 1xPBS, 6 M glycerol	1.0 (-13°C)	2.807 (-24°C)	35.9	[18]
	1.55 (-64°C)	1.993 (-74°C)		
	1.42 (-110°C)	1.152 (-110°C)		
	1.24 (-148°C)	0.809 (-148°C)		
Porcine Liver treated with 1xPBS, 8 M glycerol	0.65 (-10°C)	2.688 (-23°C)	40.1	[18]
	1.27 (-64°C)	1.969 (-75°C)		
	1.07 (-109°C)	1.19 (-111°C)		
	0.86 (-149°C)	0.781 (-148°C)		